JOURNAL OF INFORMATION SCIENCE AND ENGINEERING 23, 299-313 (2007)

Short Paper

Recognize Aircraft in ISAR Images

TSORNG-LIN CHIA, SHEN-CHI TIEN* AND YIBIN LU*
Department of Computer and Communication Engineering
Ming Chuan University
Taoyuan, 333 Taiwan
**Department of Electrical Engineering*
Chung Cheng Institute of Technology
National Defense University
Taoyuan, 335 Taiwan

This paper provides a novel method to recognize aircraft in Inverse Synthetic Aperture Radar (ISAR) images. The method utilizes the conspicuous scatterers located in a two-dimensional ISAR image as the feature points of aircraft to generate geometric invariants and recognize the aircraft. When the ISAR imagery is influenced by noise or target rotation, the proposed method provides an effective recognition. To alleviate the computational complexity, the ordered geometric invariants and the primary key are employed. Moreover, dynamic thresholds are applied to increase the accuracy of feature comparisons. The experimental results show that the proposed method is robust and effective to identify aircraft in ISAR images.

Keywords: ISAR image, scatterer, point-scatterer model, cross-ratio, aircraft recognition

1. INTRODUCTION

Inverse Synthetic Aperture Radar (ISAR) is a version of SAR that can be used operationally to image targets such as ships, aircraft, and space objects. In ISAR, the radar is stationary (or moving) while the target to be imaged is moving in a noncooperative way. Fig. 1 illustrates the ISAR geometry. ISAR imagery is generated from reflectively data collected as the target rotates while remaining in the radar beam. The direction of radar line-of-sight (LOS) is referred as to range, and the direction orthogonal to range is referred to as cross-range [1]. Since the two-dimensional (2D) radar image can be provided in all-weather, day and night, ISAR is suitable for some applications where utilizing optical equipment are disadvantageous at traffic control and surveillance systems. For example, ISAR images are applied to the near-range radar network (NRN) for traffic guidance and control on airport surfaces [2] and the automatic aircraft landing (AAL) system [3]. Target classification or recognition is an important work in these systems, which can aid operators to execute accurate decision and process in the system. Although

Received November 22, 2004; revised April 25 & August 18, 2005; accepted November 3, 2005.
Communicated by Kuo-Chin Fan.

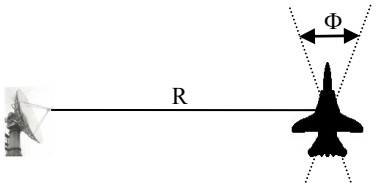

Fig. 1. ISAR geometry. The radar is stationary and the target rotates through an angle Φ in a range R.

radar systems provide all-weather representations of the detected objects with good resolution, clutter and noise can degrade the overall performance of the automatic target recognition (ATR) system significantly. Therefore, some approaches exploit the scattering characteristics in ISAR images to classify ships or aircraft. Musman and Keer [4] utilize the 2D ISAR images to classification ships, but the method need store the wire-frame models of ships for comparison. Botha *et al.* [5] use a feedforward neural net as classifier to identify non- cooperative aircraft in 2D ISAR images. Hudson and D. Psaltis [6] perform target recognition based on the one-dimensional (1D) range profile. However, the amplitude of the received backscatter from a scattering point could have a dramatic change as the aspect angle is altered.

In this paper, the proposed method for recognizing aircraft applies primarily to those aircraft detected at far range from the ISAR, and ISAR imagery of aircraft is limited to have dimensions that are small compared with both aircraft range to the radar and cross-range extent of the radar antenna beam. Therefore, the feature points extracted from ISAR images are regarded as coplanar features that are projected on a 2D image. In an ISAR image, conspicuous scatterers are mainly produced by specular and diffractive scattering mechanism [7], and these scatterers are regarded as the object's projection on the LOS of the radar. Fig. 2 shows a sketch map of scatterers of an aircraft in an ISAR image. Since the distinguishable scatterers in an ISAR image typically appear at constant locations [8, 9], the proposed recognition method employs these scatterers and the geometric relationships among them to generate a set geometric invariants and to recognize an aircraft in ISAR images. When the conspicuous scatterers are extracted from an ISAR image, three-dimensional (3D) aircraft recognition is translated into a matching features problem in an image plane consequently. As viewing at a known angle, projective features in an image plane were used according to a 2D-2D points matching method to match two sets of points [10, 11]. These 2D-2D point matching methods use a speedy searching algorithm, which takes advantage of the relative distance between each pair of points, to examine all possible matching and determine an optimal solution. However,

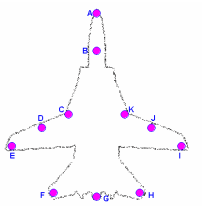

Fig. 2. A sketch map of scatterers in an ISAR image.

the object scale influences the calculated distances among points in an image, causing the matching errors.

To design an efficient aircraft recognition method, we must obtain robust features that are insensitive to the radar-target orientation and noise contamination, while keeping sufficient class separability between targets. Moreover, the dimension of the extracted feature vectors should be small in order to reduce the computational burden in the classifier stage. Thus, the extracted feature points (scatterers) are used to form a set of geometric invariants – cross-ratios [12-14] that act as the model bases for recognizing aircraft in a ISAR image. Cross-ratios are not influenced by the translation, rotation, scaling transformations and the viewpoint altered. However, the calculated cross-ratios for the extracted scatterers are real-value numbers, and the range of cross-ratios is a non-uniform distribution. Though the recognition can use these real numbers to match features, defining a fixed and reasonable threshold to restrict matching errors is difficult. Consequently, an approach that transfers real cross-ratios to integral cross-ratios is proposed and described in section 3. The approach generates a set of integral cross-ratios with uniform distribution to represent aircraft. Using the integral cross-ratios enhances the tolerance of the calculated error and increases the convenience of matching features. Furthermore, the aircraft model formed by the integral cross-ratios is only a string of integral numbers, so the complexity of searching the database and comparing model data decreases dramatically.

This paper is arranged as follows. Section 2 elucidates the method of extracting and ordering scatterers, the theory of cross-ratios and the descriptions of aircraft models. The procedure for establishing the model database and the algorithm of matching features are described in section 3. Section 4 addresses the stability analysis of cross-ratios. Section 5 presents experiments and results obtained using simulated scatterers. The final section offers a conclusion.

2. AIRCRAFT REPRESENTATION IN ISAR IMAGES

2.1 Feature Points Extraction

Since the scatterers present in an ISAR image are reflectivity magnitude associated with the illuminated target, we get the conspicuous feature points through adequate segmentation in an ISAR image. According to the reflectivity magnitude in the ISAR image, a threshold can be determined for image segmentation. Several regions whose reflectivity magnitude is larger than the threshold are extracted from the segment results. Then, the centroid of each segmented region is defined as the scatterer location in the ISAR image. Nevertheless, the segment results will be influenced by the threshold and the scale of the projective ISAR image. Hence, a dynamic threshold is employed to produce a finite set of scatterer regions (k) after the segment processing. The threshold value is determined according to the decided number of the extracted regions in the segmentation. Assuming the maximum and minimum magnitudes in an ISAR image are $M_{\max}$ and $M_{\min}$, respectively. The threshold (T) is set equal to $M_{\max}/2$ firstly, and the ISAR image is segmented using the threshold. The segment processing runs in the following steps to extract a finite set of scatterer regions (k).

(a) $T_h = M_{\max}$, $T_l = M_{\min}$;
(b) Segment the ISAR image by the threshold T and obtain k' scatterer regions;
(c) If the number of extracted regions (k') is equal to k, the segmentation is completed. Otherwise, the threshold is adjusted using the following method.
If $k' > k$, set $T_l = T$, and $T = T + (T_h - T)/2$; go to step (b).
If $k' < k$, set $T_h = T$, and $T = T + (T - T_l)/2$; go to step (b).

The positions and strengths of object scatterers can be determined from the reflected pulse signals since the object imagery is formed by reflected radar pulses in a radar image. Therefore, the point-scatterer model approximately describes the scattering distribution of the real ISAR image [15-17], and it is applied here to simulate the scattering distribution. Since the location of the nose scatterer (labeled A in Fig. 2) can be determined from the motion between the radar and the moving object, the locations of other scatterers can be determined by employing an ordering procedure. The ordering procedure is described as follows. (Supposing k points of scatterers after the segment processing, and the positions of scatterers are (x_i, y_i), $i = 1, 2, \ldots, k$)

(a) Calculate the centroid of all scatterer locations in the image plane,

$$(x_c, y_c) = \frac{1}{k}\sum_{i=1}^{k}(x_i, y_i).$$

(b) Calculate the length of the connection from the centroid to each scatterer and the angle (θ_{ci}) between the line formed by the centroid and the nose scatterer and the line of connection, where $\theta_{ci} \in [0°, 360°)$, $i = 1, 2, \ldots, k$.
(c) Sort the angles, θ_{ci}, counterclockwise to generate the order of the scatterers. If two or more scatterers have the same angle, then connect the scatterer of the longer length in advance of the shorter length.

Next, the order scatterers are used to calculate a set of integral cross-ratios, which form a cross-ratio vector to represent an aircraft in an ISAR image.

2.2 Cross-ratio Definition

A target object in a 3D space scanned by radar pulses forms a projection in a 2D image, and the extracted features are regarded as the vertices of the polygonal object, *abcde*, as shown in Fig. 3. The lines that connect vertex a to the other four vertices, b, c, d, e, intersect line L at four points, p_1, p_2, p_3, p_4, respectively. The cross-ratio formed by four points, p_1, p_2, p_3, p_4, on the line L is defined as

$$CR_L(p_1, p_2, p_3, p_4) = \frac{\left|\overline{p_1 p_3}\right| \cdot \left|\overline{p_2 p_4}\right|}{\left|\overline{p_2 p_3}\right| \cdot \left|\overline{p_1 p_4}\right|}. \tag{1}$$

Taking the vertex a of the polygonal object as a focal point, the angular definition of the cross-ratio is

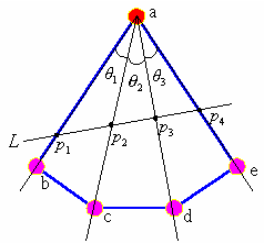

Fig. 3. The geometric relationship of scatterers to form a polygonal and calculate cross-ratios.

$$CR_a(\theta_1, \theta_2, \theta_3) = \frac{\sin(\theta_1 + \theta_2) \cdot \sin(\theta_2 + \theta_3)}{\sin(\theta_2) \cdot \sin(\theta_1 + \theta_2 + \theta_3)}, \tag{2}$$

and the following relationship is obtained and proven in [12],

$$CR_L(p_1, p_2, p_3, p_4) = CR_a(\theta_1, \theta_2, \theta_3). \tag{3}$$

Since the cross-ratio has the invariant property in projective geometry, its value is invariant under translation, rotation, and scaling transformations or various viewpoints. Therefore, cross-ratios are employed as features and formed a feature vector – a cross-ratio vector, acting as a model for recognizing the object in ISAR images.

2.3 Aircraft Descriptions

The geometric relationships of scatterers are utilized to calculate a set of cross-ratios to represent an aircraft in an ISAR image and conquer the translation, rotation, and scale of the aircraft or the influences of noise. Moreover, the computing method of the cross-ratios of aircraft uses pre-defined geometric relationships among scatterers since the outlines of aircraft are almost similar to each and belonged to a symmetrical structure. Two types of cross-ratios are employed to describe an aircraft, and the calculated methods are described as follows.

(a) Outline Description (OD): The most salient scatterers of the aircraft's shape, that include the locations of nose, wing and tail tip (scatterers A, C, E, F, G), are used to form a convex polygon shown in Fig. 4. These five scatterers are applied to calculate a set of cross-ratios, called the *outline description cross-ratios*. Since the aircraft is a symmetrical structure, the cross-ratios calculated using the scatterers A, C, E, F, G are similar to the cross-ratios calculated using the scatterers A, K, I, H, G. The second set cross-ratios can be used to replace the first set cross-ratios in matching process while the matching is unknown in the database. Hence, five cross-ratios are adopted and the formulas of these cross-ratios according to Eq. (2) are

$$OD_1 = CR(A,C,E,F,G) = \frac{\sin(\angle EAC + \angle CAF) \cdot \sin(\angle CAF + \angle FAG)}{\sin(\angle CAF) \cdot \sin(\angle EAC + \angle CAF + \angle FAG)} = CR(A,K,I,H,G) = OD'_1, \tag{4}$$

$$OD_2 = CR(C,E,F,G,A) = \frac{\sin(\angle ECF + \angle FCG) \cdot \sin(\angle FCG + \angle GCA)}{\sin(\angle FCG) \cdot \sin(\angle ECF + \angle FCG + \angle GCA)} = CR(K,I,H,G,A) = OD'_2, \tag{5}$$

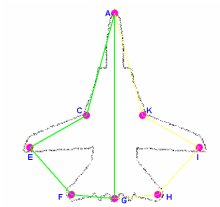

Fig. 4. The geometrical relationship of the outline description cross-ratios. The (green) polygon illustrates the geometrical relationships of *OD*, and the (yellow) dot-line polygon shows the geometrical relationships of *OD*′.

$$OD_3 = CR(E,F,G,A,C) = \frac{\sin(\angle FEG + \angle GEC)\cdot\sin(\angle GEC + \angle AEC)}{\sin(\angle GEC)\cdot\sin(\angle FEC + \angle GEC + \angle AEC)} = CR(I,H,G,A,K) = OD'_3, \quad (6)$$

$$OD_4 = CR(F,G,A,C,E) = \frac{\sin(\angle GFA + \angle AFC)\cdot\sin(\angle AFC + \angle CFE)}{\sin(\angle AFC)\cdot\sin(\angle CFA + \angle AFC + \angle CFE)} = CR(H,G,A,K,I) = OD'_4, \quad (7)$$

$$OD_5 = CR(G,A,C,E,F) = \frac{\sin(\angle AGC + \angle CGE)\cdot\sin(\angle CGE + \angle EGF)}{\sin(\angle CGE)\cdot\sin(\angle AGC + \angle CGE + \angle EGF)} = CR(G,A,K,I,H) = OD'_5. \quad (8)$$

(b) Wing Description (WD): The scatterers produced at the locations of wing and tail tips and cockpit bulkhead (scatterers C, D, E, F, H, I, J, K), as shown in Fig. 5, are used to compute three cross-ratios, called the *wing description cross-ratios*. These cross-ratios are calculated by the following formulas. The *WD* cross-ratios can be replaced by *WD*′ cross-ratios in the matching process to increase the recognition rate.

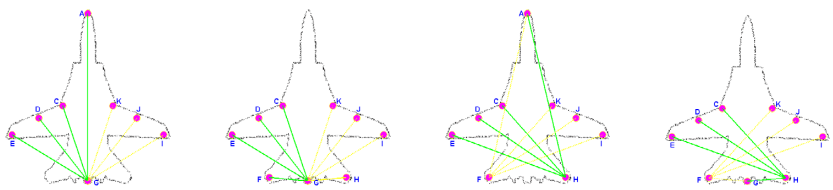

(WD_1) (WD_2) (WD_3) (WD_4)

Fig. 5. The geometrical relationship of the wing description cross-ratios. The (green) lines illustrate the geometrical relationships of *WD*, and the (yellow) dot lines show the geometrical relationships of *WD*'.

$$WD_1 = CR(G,A,C,D,E) = \frac{\sin(\angle AGC + \angle CGD)\cdot\sin(\angle CGD + \angle DGE)}{\sin(\angle CGD)\cdot\sin(\angle CGD + \angle CGD + \angle DGE)} = CR(G,A,K,J,I) = WD'_1 \quad (9)$$

$$WD_2 = CR(G,C,D,E,F) = \frac{\sin(\angle CGD + \angle DGE)\cdot\sin(\angle DGE + \angle EGF)}{\sin(\angle DGE)\cdot\sin(\angle CGD + \angle DGE + \angle EGF)} = CR(G,K,J,I,H) = WD'_2 \quad (10)$$

$$WD_3 = CR(H,A,C,D,E) = \frac{\sin(\angle AHC + \angle CHD)\cdot\sin(\angle CHD + \angle DHE)}{\sin(\angle CHD)\cdot\sin(\angle AHC + \angle CHD + \angle DHE)} = CR(F,A,K,J,I) = WD'_3 \quad (11)$$

$$WD_4 = CR(H,C,D,E,G) = \frac{\sin(\angle CHD + \angle DHE)\cdot\sin(\angle DHE + \angle EHG)}{\sin(\angle DHE)\cdot\sin(\angle CHD + \angle DHE + \angle EHG)} = CR(F,K,J,I,G) = WD'_4 \quad (12)$$

3. DATABASE CONSTRUCTION AND DATA MATCHING

3.1 Construct a Cross-ratio Database

The cross-ratios calculated to represent scatterers are real-value numbers ($\in R$) and influenced by noise; they are therefore hard to use as a searching index in the database. Therefore, the real cross-ratios are converted to the integral cross-ratios ($\in N$) by a statistical method and formed a conversion table. This approach increases the error tolerance and facilitates in matching the integral cross-ratios. The conversion method describes as follows.

Table 1. The aircraft model descriptions in the database.

Aircraft	Model Descriptions								
	OD_1	OD_2	OD_3	OD_4	OD_5	WD_1	WD_2	WD_3	WD_4
F-14	75	78	18	94	22	31	34	38	38
F-15E	45	51	16	83	28	38	33	40	11
F-16C	67	71	16	93	21	18	51	14	71
F-18C	62	68	29	88	22	10	67	14	67
A-10	32	35	7	87	18	32	29	34	47
MIG-29	89	91	24	97	23	31	36	37	16
C-141	17	19	5	80	23	22	47	23	45
SOKOG-4	63	66	13	93	18	26	35	33	39
B-1B	75	77	16	95	19	19	46	25	39
H-6	48	52	10	90	17	32	28	38	13
B-747SP	10	11	2	86	15	35	23	37	31
MIG-19	27	28	4	90	12	31	22	34	30
MIG-21	66	70	17	92	23	25	42	30	21
A-6	29	34	10	80	26	30	41	33	29
A-7	75	76	9	97	12	26	26	32	31
SAAB-2000	28	30	6	86	18	40	23	38	43

First, the method uses Eq. (2) to calculate all cross-ratios in the constrained ranges, $0 \le \theta_1, \theta_2, \theta_3 \le \pi$ and $0 \le \theta_1 + \theta_2 + \theta_3 \le \pi$, increasing each included angle by a small increment $\Delta\theta_i$, $i = 1, 2, 3$, and analyzing the numerical distribution of the calculated results. Next, all calculated cross-ratios are divided into M parts, and the probability that a cross-ratio occurs in the Mth portion is considered the same for all cross-ratios. Finally, the range of integral cross-ratios is set to 1-M, and the real cross-ratios are converted to integral cross-ratios according to the conversion table. The cross-ratios described in below are integral cross-ratios. According to the definitions of cross-ratios described in section 2, each aircraft model is represented by a vector of nine cross-ratios. These cross- ratio vectors are collected to form a database for aircraft recognition, and the database is shown in Table 1. The format includes five outline description cross-ratios and four wing description cross-ratios.

3.2 Cross-Ratios Matching

Each aircraft model has eight cross-ratios in the database, and the cross-ratios matching can compare the cross-ratios of the tested model with that of each model in the database intuitively. However, this method consumes the comparison time dramatically when the number of aircraft models increases greatly. Therefore, the matching method needs to exclude those impossible aircraft model first to decrease the comparing cost. A primary key, having the fine discriminability and stability among the cross-ratio descriptions of aircraft models, is applied to decrease the searching time of the database. A criterion is utilized to select the primary key from the cross-ratio descriptions and deduced in section 4. Moreover, if the value of a cross-ratio description distributes over a large range, the cross-ratio description provides a fine discriminability. Hence, the standard deviation of the cross-ratio descriptions is used as a threshold in the database searching. As the value of the primary key of the tested model compares with that of the model in the database below the threshold, the model data is used to compare with the descriptions of the tested aircraft. Furthermore, some cross-ratios of aircraft descriptions may produce approximate cross-ratios when aircraft models increase, and the similar cross-ratios will easily cause the matching error. If the noise margin of each cross-ratio description is not large enough, the recognizing method is difficult to identify an aircraft in the large database. Similarly, if the matching threshold of each cross-ratio description is set to a fixed value, the recognizing results may produce multiple models coinciding with the tested model. Thus, various thresholds of each cross-ratio description are employed to solve these problems, and these thresholds are generated by the standard deviation of each cross-ratio description in the database.

Suppose that the number of the cross-ratios of i-th aircraft model is m, and the m-dimensional vector, P_i, is represented as (D_{i1}, D_{i2}, …, D_{im}) and its similar feature calculated using the symmetrical structure of the aircraft is represented as (D'_{i1}, D'_{i2}, …, D'_{im}). The built database has n aircraft models for recognition. According to the order of the cross-ratio vector, the comparison of the j-th cross-ratio between the tested aircraft and the database model is defined as

$$T_{ij} = (C_{ij}^1, C_{ij}^2, ..., C_{ij}^n) \bullet T_{i,j-1}, \; j = 1, 2, \ldots, m; \tag{13}$$

where C_{ij}^k represents the matching result of the j-th cross-ratio between the tested aircraft P_i and the k-th model in the database and is defined as

$$C_{ij}^k = \begin{cases} 1, & |D_{ij} - D_{kj}| \le \lambda_j \text{ or } |D_{ij} - D'_{kj}| \le \lambda_j \\ 0, & \text{otherwise} \end{cases}, \; k = 1, 2, \ldots, n. \tag{14}$$

λ_j represents the threshold of the j-th cross-ratio description and deduces from the standard deviation of the cross-ratio descriptions in the database to form a threshold vector, λ. In addition, T_{ij} is the matching result between the tested model and the database models, and its initial state is set as T_{i0} = (1, 1, …, 1). The operator "•" in Eq. (13) represents a logical AND operation. Finally, three types of the matching results are given when the comparisons of cross-ratios are accomplished, and described as follows.

(a) Correct: Only one component, C_{ij}^{k}, among the matching result, T_{ij}, exists a non-zero value and the tested aircraft is determined as the k-th model of the database.
(b) Uncertain: The uncertain recognition includes two cases, reject and unknown. One, the case of reject, all components of the matching result become zeros, $T_{ij} = (0, 0, \ldots, 0)$, occur either in processing or at finish of the comparisons, and this result shows that the tested model is not contained in the database. The other, the case of unknown, C_{ij}^{k}, exists many non-zero values among the matching result, T_{ij}, at the comparisons finished, and this result is unable to determine the tested model from the database models.
(c) Inaccurate: The matching result appears only one non-zero value in T_{ij}, but it is not the model number of the tested aircraft.

4. STABILITY ANALYSIS OF CROSS-RATIO

The displacements of scatterers, influenced by noise or the extracted thresholds, may vary the cross-ratio since the calculated cross-ratio is formed by five scatterers. Therefore, the real cross-ratios are converted into integral cross-ratios to increase the error tolerance in matching cross-ratios. However, cross-ratios may be greatly varied by a large variance of noise. Consequently, a searching key is provided for searching data in the database, and this approach can reduce the costs of searching the database and matching data.

The analysis method of Song *et al.* [14] is followed to derive a criterion for selecting a searching key, such that the selected key is suitable for the recognition method. Supposing that the cross-ratio of five scatterers is τ, Eq. (2), $CR_a(\theta_1, \theta_2, \theta_3) = \tau$, can be represented by the following formula (Ref. to Fig. 2).

$$\tau = \frac{\frac{1}{2}\left|\overline{ab}\right|\left|\overline{ad}\right|\sin(\theta_1+\theta_2)\cdot\frac{1}{2}\left|\overline{ac}\right|\left|\overline{ae}\right|\sin(\theta_2+\theta_3)}{\frac{1}{2}\left|\overline{ac}\right|\left|\overline{ad}\right|\sin(\theta_2)\cdot\frac{1}{2}\left|\overline{ab}\right|\left|\overline{ae}\right|\sin(\theta_1+\theta_2+\theta_3)} = \frac{S_1S_2}{S_3S_4}, \tag{15}$$

where $S_i = \frac{1}{2}A_iB_i\sin(\Theta_i)$, $i = 1, 2, 3, 4$ is the area of the triangle, and A_i, B_i are the lengths of the two edges adjacent to the including angle Θ_i. The corresponding relationships between Eq. (15) and S_i are $(A_1, B_1) = (\left|\overline{ab}\right|, \left|\overline{ad}\right|)$, $\Theta_1 = \theta_1 + \theta_2$; $(A_2, B_2) = (\left|\overline{ac}\right|, \left|\overline{ae}\right|)$, $\Theta_2 = \theta_2 + \theta_3$; $(A_3, B_3) = (\left|\overline{ac}\right|, \left|\overline{ad}\right|)$, $\Theta_3 = \theta_2$; $(A_4, B_4) = (\left|\overline{ab}\right|, \left|\overline{ae}\right|)$, $\Theta_4 = \theta_1 + \theta_2 + \theta_3$.

The error rate of the cross-ratio influenced by noise or displacement is defined as $ER = |\Delta\tau/\tau|$, where $\Delta\tau$ is the variance of the cross-ratio. Then, differentiating Eq. (15) yields

$$\partial\tau = \frac{S_2}{S_3S_4}\partial S_1 + \frac{S_1}{S_3S_4}\partial S_2 - \frac{S_1S_2}{S_3^2S_4}\partial S_3 - \frac{S_1S_2}{S_3S_4^2}\partial S_4, \tag{16}$$

and substituting Eqs. (15) and (16) into ER yields

$$ER \cong \left|\frac{\Delta S_3}{S_3} + \frac{\Delta S_4}{S_4} - \frac{\Delta S_1}{S_1} - \frac{\Delta S_2}{S_2}\right|. \tag{17}$$

This equation shows that the error rate of the cross-ratio is a function of the variation of the measured area of the triangle. Differentiating S_i yields,

$$\partial S_i = \frac{1}{2}(B_i \sin\Theta_i \cdot \partial A_i + A_i \sin\Theta_i \cdot \partial B_i + A_i B_i \cos\Theta_i \cdot \partial\Theta_i), \tag{18}$$

and

$$\frac{\Delta S_i}{S_i} \cong \frac{\Delta A_i}{A_i} + \frac{\Delta B_i}{B_i} + \frac{\Delta\Theta_i}{\tan\Theta_i}, \tag{19}$$

where the variation of $\Delta\Theta_i$ is also affected by the vertex displacements of the two adjacent edges, and the maximum variation of $\Delta\Theta_i$ is

$$\Delta\Theta_i \cong \frac{\Delta A_i}{A_i} + \frac{\Delta B_i}{B_i}, \tag{20}$$

such that,

$$\frac{\Delta S_i}{S_i} \cong \left(1 + \frac{1}{\tan\Theta_i}\right)\left(\frac{\Delta A_i}{A_i} + \frac{\Delta B_i}{B_i}\right). \tag{21}$$

Finally, let $D = \left(1 + \frac{1}{\tan\Theta_i}\right)\left(\frac{1}{A_i} + \frac{1}{B_i}\right)$, $i = 1, 2, 3, 4$ and the criterion of the searching keys is specified as

$$SK = \left| D_3 + D_4 - D_1 - D_2 \right|. \tag{22}$$

A smaller *SK* corresponds to a more stable cross-ratio and represents the fact that the variation of the cross-ratio is hardly influenced by noise or the displacements of scatterers. Therefore, a stable cross-ratio description is selected as the searching key when the database is established to accelerate the comparison of the data. Eq. (22) is used to select the searching key, the cross-ratio description with the smallest *SK*, in the database.

5. EXPERIMENTAL RESULTS

Since ISAR technology is still at the research and design stage, and only a few experimental systems are reported under development in the literature [18]. Most researchers used synthetic ISAR images or models to demonstrate their proposed methods in ISAR technology [15, 16]. Since the recognition method in ISAR imagery is mainly discussed in this paper, the synthetic ISAR data are used to demonstrate the proposed method. The conspicuous scatterers in an ISAR image typically appear at constant locations [8, 9], and the segment procedure will not be demonstrated in experiments. Nevertheless, the scatterer positions are added different variance (Gaussian) noise to simulate the positions variation after segment processing in the experiments. Suppose that the conspicuous scatterers have extracted and ordered using the procedures elucidated in section 2.1, and the locations of scatterers of all aircraft models are pre-defined in experiments. Aircraft models are established by the simulated scatterers and Fig. 6 shows

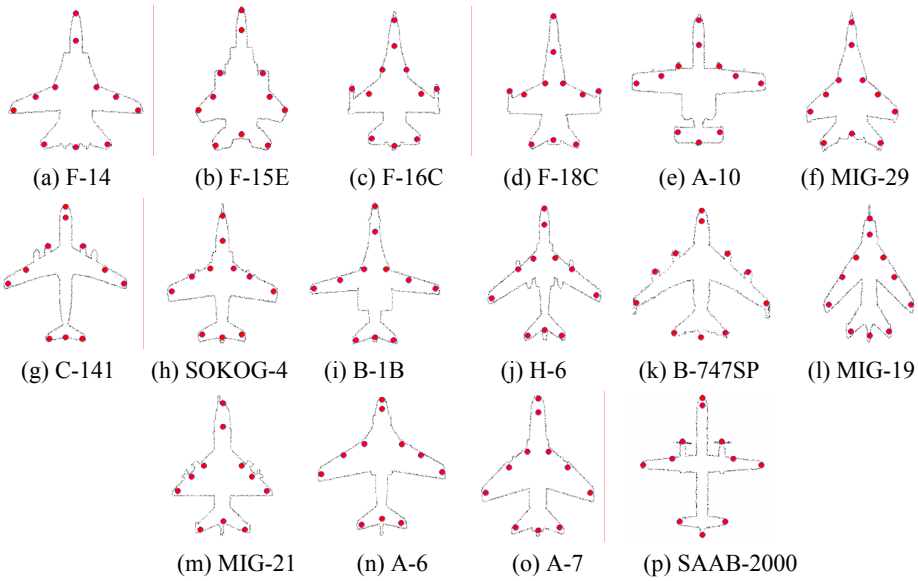

Fig. 6. The sketch map of aircraft models in the database.

the point-scatterer models of aircraft in the database. According to the recognition method elucidated in section 3, we constitutes a database that is based on cross-ratios for recognizing an aircraft model in an ISAR image, as shown in Table 1. Moreover, the primary key selected by Eq. (22) is the second cross-ratio of the wing description, WD_5, and the searching threshold is set to $s = 5$ for selecting the model's data in the database.

In recognizing a tested aircraft model, the outline description cross-ratios and wing description cross-ratios are calculated first, and then these features are compared with the model's data in the database to determine the tested aircraft model. Moreover, the matching thresholds must be set carefully, because the larger thresholds will increase the uncertain recognition and the smaller thresholds will also decrease the correct recognition. Therefore, the error tolerance of matching is set to $\lambda = \lceil 0.5 \times \text{std} \rceil$, where std is the standard deviation vector of the descriptions in the database, and get a reasonable thresholds. The threshold vector, λ, is set to (13, 13, 4, 3, 3, 4, 7, 5, 9) in all experiments. Additionally, the recognizing results are given as the percentages of correct, uncertain, and inaccurate recognition. The proportion of uncertain results from the tested model is influenced by noise with a large variance and not classified in inaccurate recognition.

First, the scatterer positions of the tested aircraft are varied by adding noise with different variances to simulate the segment results, an example F-14 is shown in Fig. 7, and then performing aircraft recognition in the database to investigate the robustness of the method. Figs. 8 (a-e) depict the percentages of the correct, uncertain, and inaccurate recognition, which each aircraft model is recognized 1,000 times as adding with different variances noise to the scatterer positions. The percentages of the correct, uncertain, and inaccurate recognition of each tested model are depicted as the blue, green, and red bars, respectively. As the variance of noise is increasingly augmented, the percentage of correct recognition is decreased dramatically and the percentage of uncertain recognition

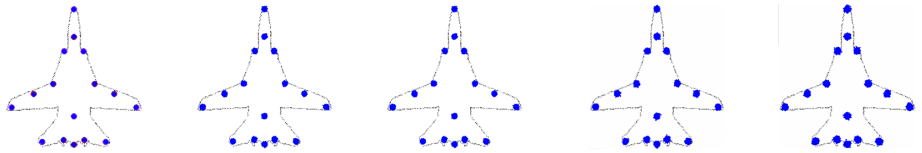

(a) $\sigma^2 = 2$ pixels^2. (b) $\sigma^2 = 4$ pixels^2. (c) $\sigma^2 = 6$ pixels^2. (d) $\sigma^2 = 8$ pixels^2. (e) $\sigma^2 = 10$ pixels^2.

Fig. 7. An example of F-14, the scatterers distribution in adding noise with different variances.

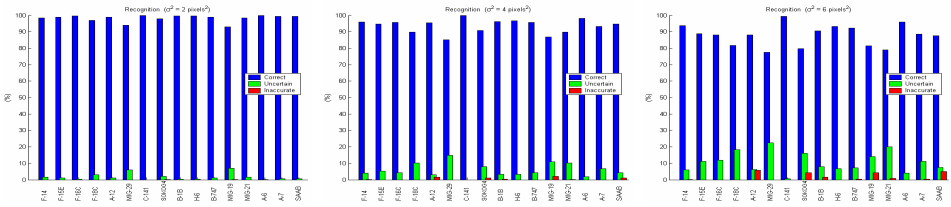

(a) $\sigma^2 = 2$ pixels^2. (b) $\sigma^2 = 4$ pixels^2. (c) $\sigma^2 = 6$ pixels^2.

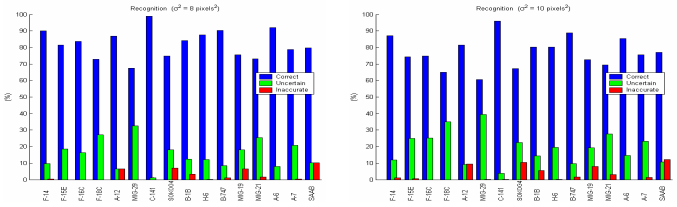

(d) $\sigma^2 = 8$ pixels^2. (e) $\sigma^2 = 10$ pixels^2.

Fig. 8. The recognition results of the scatterer positions adding noise with different variances.

is increased greatly. Still, the percentage of inaccurate recognition is lower than that of correct recognition. The percentage of correct recognition is maintained on average 77.21% in the case of adding the largest variance of noise ($\sigma^2 = 10$), whereas the inaccurate percentage of recognition is kept in the rate below average 3.36%.

Second, ISAR imagery is generated from reflectively data collected as the target rotates while remaining in the radar beam, and the scatterers is rotated to simulate the target motion and investigate the robust and effective of the recognition method. The scatterers of all models are rotated in a test range, the directions of pitch, roll and yaw are rotated different angles from – 30° to 30°, and the scatterer positions varied by noise with different variance. An example of model rotation is shown in Fig. 9 (a), and the recognition results are shown in Figs. 9 (b-f). The correct recognition is maintained on an average 73% in the case of adding the largest variance of noise, whereas the inaccurate percentage of recognition is kept in the rate below 3.96%. The recognition method is robust and effective for the aircraft rotation.

Finally, an aircraft model, F-14C, with a scatterer segmented at wrong positions as shown in Fig. 10 (a), was used to verify the robustness of the recognition method. The scatterer positions are influenced by diverse variances of Gaussian noise to perform the recognition. The experimental results, as shown in Fig. 10 (b), reveal that the correct rate and inaccurate rate is 69%-100% and 0%, respectively, when the scatterer is segmented

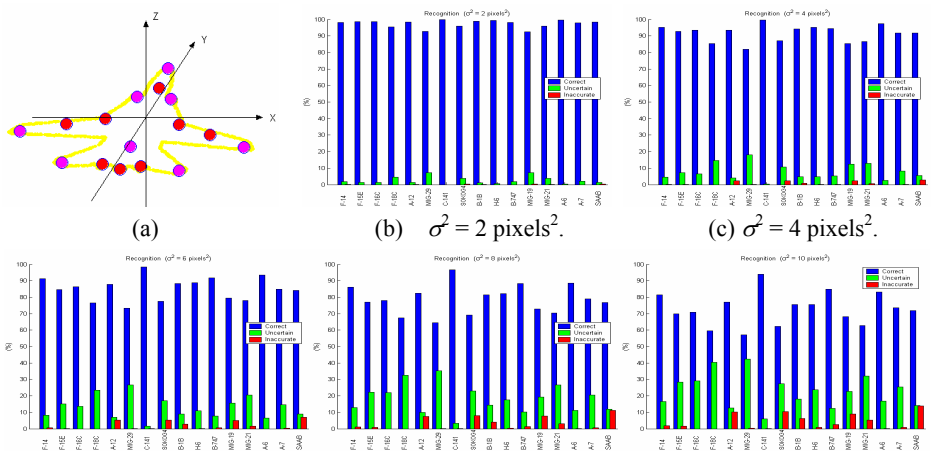

(a) (b) $\sigma^2 = 2$ pixels^2. (c) $\sigma^2 = 4$ pixels^2.

(d) $\sigma^2 = 6$ pixels^2. (e) $\sigma^2 = 8$ pixels^2. (f) $\sigma^2 = 10$ pixels^2.

Fig. 9. (a) An example depicts the point scatterers processed by rotation. (pitch = 10°, roll = 10°, yaw = 20°) The recognition results of the scatterer positions adding noise with different variances are shown in (b-f).

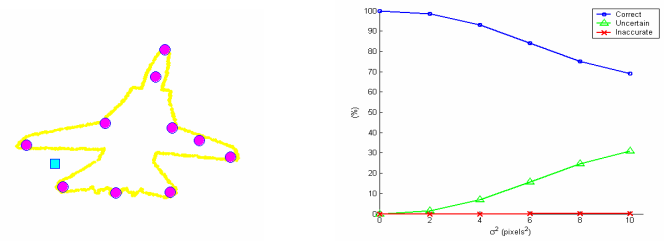

(a) (b)

Fig. 10. (a) The simulated scatterers of model F-14C, where the scatterer depicted by square is extracted at wrong position in the aircraft model; (b) The recognition results of the scatterer positions in adding noise, where the (blue) circle, (green) triangle, (red) *x*-mark curve represents the correct, uncertain and inaccurate recognition rate, respectively.

at different position of the model and varied with different variances noise. The experimental results show that the proposed method is both robust and effective in recognizing aircraft in ISAR images. Although the method was not confirmed by the real ISAR images, the simulated results showed that the recognition method should be appropriate for applications of real ISAR images.

6. CONCLUSIONS

This work presents a novel method that uses geometric invariants to identify an aircraft in an ISAR image. The method relies on the characteristic that the scatterers of the aircraft appear at fixed locations in ISAR images. The cross-ratio description of an aircraft model is a fixed and ordered vector, and a small database is built for recognition.

Furthermore, a criterion for selecting a stable key is deduced, to accelerate matching, in establishing a database. Applying the point-scatterer model in experiments shows that the method of recognition effectively identifies the tested aircraft model, when the scatterers are influenced by noise.

However, the projected scatterers are influenced by the rotation of a moving aircraft in real ISAR images. The number of features may differ, so that the method of matching either the same or different number of cross-ratios to the database models must be considered. Future research should address the improvement of the recognition rate and the identification of a moving aircraft in ISAR image sequences.

REFERENCES

1. D. L. Mensa, *High Resolution Radar Cross-Section Imaging*, Artech House, Norwood, Massachusetts, 1991.
2. K. H. Bethke, B. Rode, M. Schneider, and A. Schroth, "A novel noncooperative near -range radar network for traffic guidance and control on airport surfaces," *IEEE Transactions on Control Systems Technology*, Vol. 1, 1993, pp. 168-178.
3. K. Mecocci, G. Benelli, A. Garzelli, and S. Bottalico, "Radar image processing for ship-traffic Control," *Image and Vision Computing*, Vol. 13, 1995, pp. 119-128.
4. S. Musman and D. Keer, "Automatic recognition of ISAR ship images," *IEEE Transactions on Aerospace and Electronic Systems*, Vol. 32, 1996, pp. 1392-1404.
5. E. C. Botha, E. Barnard, and C. J. Barnard, "Feature-based classification of aerospace radar targets using neural networks," *Neural Networks*, Vol. 9, 1996, pp. 129-142.
6. S. Hudson and D. Psaltis, "Correlation filters for aircraft identification from radar range profiles," *IEEE Transactions on Aerospace Electronic Systems*, Vol. 29, 1993, pp. 741-748.
7. A. Zyweck and R. E. Bogner, "High-resolution radar imagery of the mirage III aircraft," *IEEE Transactions on Antennas and Propagation*, Vol. 42, 1994, pp. 1356-1360.
8. D. R. Wehner, *High Resolution Radar*, 2nd ed., Artech House, Norwood, Massachusetts, 1995.
9. T. Sauer and A. Schroth, "Robust range alignment algorithm via hough transform in an ISAR imaging system," *IEEE Transactions on Aerospace and Electronic Systems*, Vol. 31, 1995, pp. 1173-1177.
10. D. Lavine, B. A. Lambird, and L. N. Kanel, "Recognition of spatial point patterns," *Pattern Recognition*, Vol. 16, 1983, pp. 289-295.
11. P. M. Griffin and C. Alexopoulos, "Point pattern matching using centroid bounding," *IEEE Transactions on Systems*, *Man and Cybernetics*, Vol. 19, 1989, pp. 1274-1276.
12. G. Lei, "Recognition of planar objects in 3-D space from single perspective views using cross-ratio," *IEEE Transactions on Robotics and Automation*, Vol. 6, 1990, pp. 432-437.
13. J. L. Mundy and A. Zisserman, *Geometric Invariance in Computer Vision*, The MIT press, Cambridge, Massachusetts, 1992.
14. B. S. Song, I. D. Yun, and S. U. Lee, "A target recognition technique employing

geometric invariants," *Pattern Recognition*, Vol. 33, 2000, pp. 413-425.
15. R. Bhalla and H. Ling, "Three-dimensional scattering center extraction using the shooting and bouncing ray technique," *IEEE Transactions on Antennas and Propagation*, Vol. 44, 1996, pp. 1445-1453.
16. V. C. Chen and W. J. Miceli, "Simulation of ISAR imaging of moving targets," *IEE Proceedings of Radar*, *Sonar Navigation*, Vol. 148, 2001, pp. 160-166.
17. F. Berizzi, "ISAR imaging of targets at low elevation angles," *IEEE Transactions on Aerospace and Electronic Systems*, Vol. 37, 2001, pp. 419-434.
18. Z. S. Liu, R. Wu, and J. Li, "Complex ISAR imaging of maneuvering targets via the capon estimator," *IEEE Transactions on Signal Processing*, Vol. 47, 1999, pp. 1262-1271.

Tsorng-Lin Chia (賈叢林) received the B.S. degree in Electrical Engineering from Chung Cheng Institute of Technology, Taoyuan, Taiwan, in 1982, and the M.S. and Ph.D. degrees in Computer Science and Information Engineering from National Chiao Tung University, Hsinchu, Taiwan, in 1986 and 1993, respectively. He has been on the faculty in the Department of Electrical Engineering at Chung Cheng Institute of Technology during 1993-2000. Currently, he is a professor and director in the Department of Computer and Communication Engineering at Ming Chuan University. His research interests include image processing, pattern recognition, computer vision, and parallel algorithm and architecture.

Shen-Chi Tien (田笙志) received the B.S. degree in Electrical Engineering from the Chung Cheng Institute of Technology, Taiwan, R.O.C., in 1986, and the M.S. degree in Engineering from Brown University, Rhode Island, U.S.A., in 1993. He is current a Ph.D. candidate in the School of National Defense, Chung Cheng Institute of Technology. His research interests include image processing, pattern recognition, and computer vision.

Yibin Lu (陸儀斌) received the B.S. degree in Electrical Engineering from the Chung Cheng Institute of Technology and the M.S. degree in Control Engineering from National Chiao Tung University, Taiwan, R.O.C., in 1983 and 1987, respectively. He also received the Ph.D. degree in Electrical Engineering from the University of Southern California, Los Angeles, U.S.A., in 1994. He is currently an Associate Professor and the Director of Computer Application Laboratory in the Department of Electrical Engineering, Chung Cheng Institute of Technology. His research interests include optical computing, image signal processing, and multimedia applications.